ORIGINAL RESEARCH ARTICLE

Effect of Particle Incident Angle on the Hardness and Thermal Conductivity of Cu Coating Applied to a Cr-Zr-Cu Substrate using High-Pressure Cold Spray

Changzhuang Zhou, Chunzhi Gong, Ziyue Wang, and Xiubo Tian

Compared with other thermal spray technologies, cold spray relies on high-speed impact of solid particles. Generally, cold spray cannot deposit on surfaces that are positioned in low incident angle, so it is critical to understand the impact of incident angle to improve the properties of the coating in uneven or curved surfaces. In this work, pure Cu coatings were obliquely deposited on Cr-Zr-Cu substrates using high-pressure cold spray (CS) system. The influence of particle incident angle from 60° to 90° on the surface characteristics, mechanical properties and thermal conductivity of coating was studied. Results showed that increasing the incident angle of Cu particles resulted in a more compact coating. As the incident angle changed from 60° to 90°, the thickness of Cu coatings increased by 42.7%. The high micro-hardness exceeding 120 HV was maintained due to the low porosity and pure Cu particles deformation strengthening, which is close to that of 145 HV of Cr-Zr-Cu substrate. The thermal conductivity tests revealed that the superior thermal conductivity was obtained at incident angle of 90°. The results could be discussed in terms of the deformation modes of pure Cu particles and interface properties of the coatings.

1. Introduction

Copper alloy is widely used in transportation, electric power, electronics, automobiles and other fields due to its good machinability, electrical conductivity, thermal conductivity, fatigue resistance and corrosion resistance in complex environment (Ref 1). Taking the continuous casting technology as an example, the continuous casting mold is the key equipment of the continuous casting technology. It is usually made of copper/copper alloy plated with nickel or nickel alloy coating. In the continuous casting process of steel and aluminum, the low hardness and poor surface wear resistance are prone to scratch and other damage in the application process of copper alloys. In addition, the copper alloy has a low melting point, which is prone to adhesive wear, creep and other failures under high temperature conditions (Ref 2). In order to prolong its service life, improve its wear resistance, corrosion resistance and other properties, many scholars domestic and overseas analyze the damage of copper alloy components and use different processing technology to repair them. In general, non-thermal reinforcement remediation techniques are preferred to avoid harmful effects, including deformation, phase transfor-mation and oxidation associated with high-temperature processes such as welding and atmospheric plasma spraying (APS). One such low temperature technique is cold spraying (CS), which was invented in the 1980s by a group of scientists at the Institute of Theoretical and Applied Mechanics of the Siberian Branch of the Russian Academy of Sciences in Novosibirsk, Russia (Ref 3).

Cold spraying is a technology based on aerodynamics. The spraying temperature is lower than the melting point of the particles, and the solid particles of the sprayed material are given a high speed (300~1200 m s^{-1}) by kinetic energy of gas. Then, the solid particles impact the substrate at high speed to produce plastic deformation and then deposit on the surface of the substrate to form a coating (Ref 4). Due to its unique advantages in the forming of soft metal materials, cold spraying can not only keep the original properties of sprayed materials, but also rapidly prepare large and complex structures, so it has attracted increasingly attention from academia and industry and has broad application prospects (Ref 5–9).

There is a critical deposition velocity in cold spraying, and only when the particle impact velocity is above the critical deposition velocity, the particles can be successfully deposited on the substrate (Ref 10), but it is not always better with the higher impact velocity of the colliding particles. Schmidt found in their study that when the particle velocity is too high, the particle will have a serious erosion effect on the substrate and even break down the substrate, which is called erosion velocity (Ref 11). The critical deposition rate is related to the material. The material with low melting point and good plasticity is easier to deposit, indicating that the critical deposition rate is lower, while the material with poor plasticity is not easy to deposit, indicating that the critical velocity is higher (Ref 12). So far, a variety of metallic particles including Cu (Ref 13), Al (Ref 14, 15), Inconel 718 (Ref 16, 17), Ni (Ref 18), and Ti (Ref

Changzhuang Zhou, Chunzhi Gong, Ziyue Wang, and **Xiubo Tian**, State Key Laboratory of Advanced Welding and Joining, Harbin Institute of Technology, Harbin 150001, China. Contact e-mail: chunzhigong@163.com.

19, 20) have been deposited on substrate made of the same or different materials by cold spraying.

As a pioneer material of cold spraying, copper provides a lot of experimental basis for explaining the bonding mechanism. The research on cold spraying copper technology also plays an important role in guiding other materials. At present, a large number of studies show that nozzle parameters, accelerating gas parameters and powder parameters are the main factors affecting particle acceleration (Ref 21). It has been observed that the particle velocity and the collision temperature increase significantly with gas pressure and gas temperature increasing, which significantly increases the deposition efficiency of particles and the quality of coating. The size, morphology and oxygen content of powder have also significant effects on the deposition characteristics and coating quality (Ref 22–24).

However, in order to spray onto actual parts for structural repair applications, it is necessary to understand the effects of abnormal spraying on the curved or uneven surface of the actual part. Copper powder was sprayed by the cold spraying. It is found that coating deposition efficiency was supposed to increase with particle velocity and decrease strongly with gun-substrate angle, and there did not appear to be contact of the deposition efficiency on coating thickness for this system. Ni particles were deposited onto stainless steel by cold spray with different angles (Ref 25), and the substrate hardness is found to play an important role in the formation of metallurgical bonding. It is found that the maximum adhesion in the case of Ni/stainless steel decreases with the decreasing kinetic impact energy.

However, most of the current studies focus on the interface between the coating and the substrate, while few studies focus on the internal changes of the whole coating. Because the pure copper coating after cold spraying has similar hardness, wear resistance and thermal conductivity with the alloy, and the cost of pure copper powder is much lower than the alloy raw material. In this work, pure Cu coatings were obliquely deposited on Cr-Zr-Cu substrates with high-pressure cold spray (CS) technology. The effect of particles incident angle in a range of 60° to 90° on the interface and surface characteristics, mechanical and thermal conductivity behavior of the whole coatings were focused. In addition, the influence of incident angle on the deformation behavior of the powder, and the development of residual stress in CS deposition Cr-Zr-Cu were investigated.
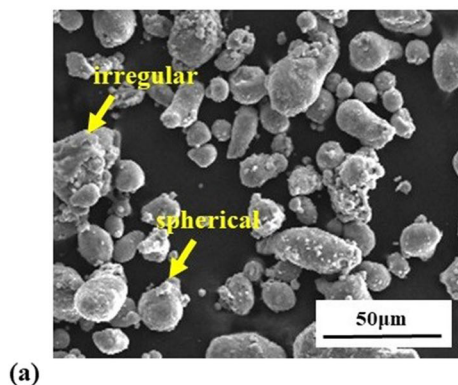
2. Materials and Methods

2.1 Material

The as-received water-atomized pure Cu powders (Beijing United Coating technologies Co., Ltd, China) were used as the cold spraying powder materials. The scanning electron microscope (SEM) images of pure Cu feedstock are shown in Fig. 1 (measured by laser particle sizer-Hydro 2000MU). It can be seen that the Cu powder presents approximately spherical and irregular shapes and is partially agglomerated. As commonly used functional copper alloy, Cr-Zr-Cu substrate was used as substrate materials (diameter of 30 mm, thickness of 5 mm) for the cold spray deposition.

2.2 Cold Spraying

Commercially available Cr-Zr-Cu alloy substrate was prepared by initially cleaning with acetone and subsequently sandblasting using SiO_2 girt to remove the oxide layer. A high-pressure PCS-100 cold spray system (Plasma Giken Co., Ltd., Japan) was used for powder deposition. Nitrogen was used as the carrier gas as well as the propelling gas. The nozzle traverse speed was set as 200 mm/s and a constant the spray distance of 25 mm was maintained throughout the deposition process with 5 spraying layers. The powder feed rate was fixed at 1 rad/min for all experiments for different impacting angles 60º, 70º, 80º, 90º. The schematic diagram of cold spray processing is shown in Fig. 2.

2.3 Characterization Procedures

2.3.1 Microstructure. The samples were cut into 10 × 10 mm with a thickness of 3 mm (coating + substrate), and the coating surface was polished and smoothed for testing. For all microstructural characterizations, samples were cross-sectioned, hot mounted in resin, ground and polished to follow standard metallurgical preparations. The cross-sectional microstructures of the coatings were observed using a scanning electron microscope (SEM, TESCAN AMBER, Harbin, China) including energy-dispersive x-ray spectroscopy (EDS). Then, the porosity was evaluated using Image-Pro Plus image analysis software. The coating crystallinity was examined using Bruker D8 Advance x-ray diffraction (XRD) with CuKα x-ray (λ = 1.54 Å) at a voltage of 40 kV and a current of
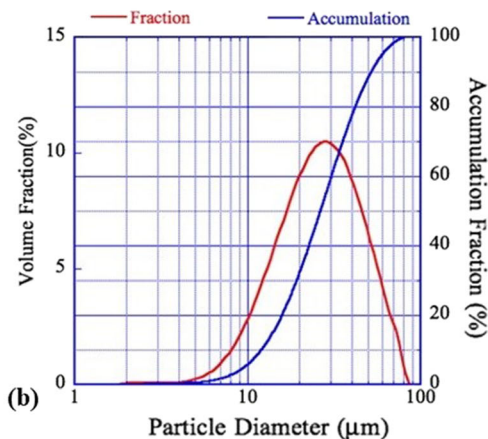

Fig. 1 (a) Particle morphology of pure copper powder. (b) Volume fraction and accumulation fraction of pure copper powder particle diameter
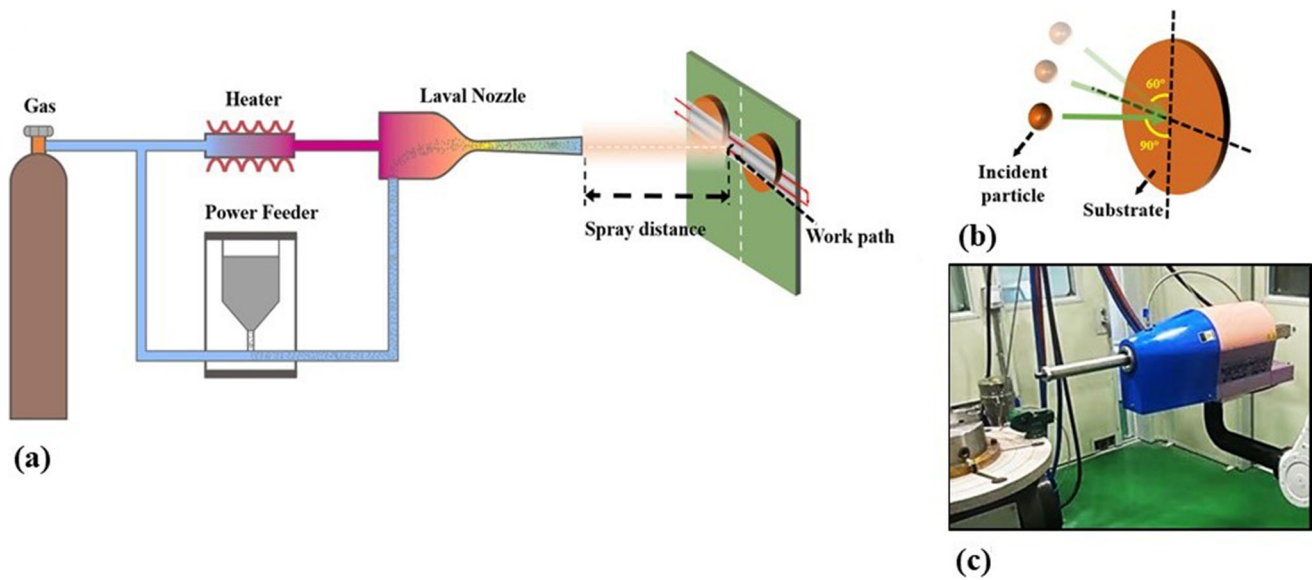
Fig. 2 (a) Schematic diagram of cold spray. (b) A schematic showing cold spray deposition setup when the nozzle was positioned at 90 and 60º to the underlying substrate. (c) Cold spray experiment equipment diagram
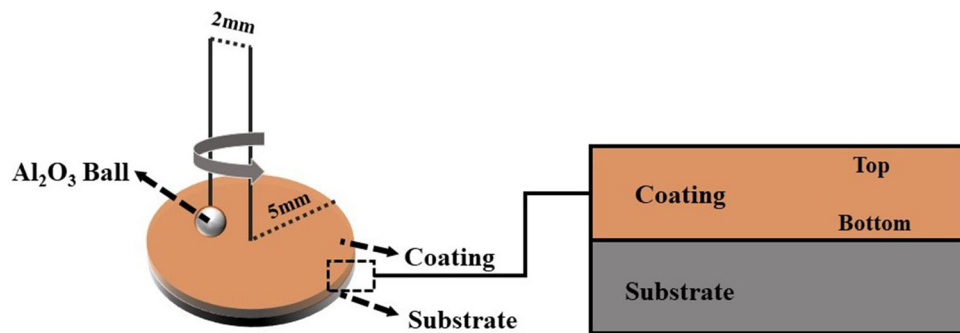

Fig. 3 Schematic diagram of the wear testing

40 mA, and coating surface residual stress was measured with CuKα x-ray using Stresstech X stress G3 x-ray stress measurement in the vertical directions of scanning path. The grain orientation and deformation strain of coating surface were observed by electron backscattering diffraction (EBSD) analysis using JEOL IT500HR FE-SEM equipped with Oxford Instruments Symmetry EBSD detector at scanning step sizes of 0.15 μm.

2.3.2 Hardness. Vickers hardness tests were done with a digital micro-hardness tester (HXD-1000TM, Shanghai optical instruments Co, Ltd., China) in the direction parallel to and perpendicular to the interface (loading 500 g, load time 15 s). Hardness analysis was measured at 25-μm intervals in the vertical interface direction, $\pm$ 100 μm from the interface. Agilent Nano Indenter G200 was used to measure hardness and modulus of cross-section surfaces with the depth at 500 nm. The average nano-hardness was determined based on five micro-zones at the different areas of the cross-sectional coating.

2.3.3 Wear Testing. As Fig. 3 shows, the samples were cut into a wafer with a diameter of 10 mm and a thickness of 3 mm (coating + substrate), and the coating surface was polished and smoothed for testing. The wear resistance of the

coating was tested by friction testing machine (T3001, Harbin, China). The friction pair was Al$_2$O$_3$. The wear radius was 2 mm. The test time was 60 min. The rotating speed was 200 r/ min, and the load was 1000 g. The wear amount was measured by a surface profiler (T3001 friction tester). The measurement of different areas (top or bottom) of the coating is achieved according to the different grinding thickness using emery paper.

2.3.4 Thermal Conductivity Testing. Apparatus LFA457 was used to measure the coating thermal conductivity of 25 and 100 °C. In light of the Cu coating is thin, we choose the measurement method of coating combined with the substrate (A wafer with a diameter of 12.7 mm and a thickness of 0.2 mm) to compare with the Cr-Zr-Cu substrate. The combination includes the Cu coating completely. At least five points were taken in each sample to measure the thermal conductivity and take the average value, and the error bar was obtained.

3. Results and Discussion

The morphologies of Cu coatings surface with different particles incident angle are shown in Fig. 4. The coating surface

consists of parts of irregularly shaped and spherical pure Cu particles. Since there was no subsequent impact of powder particles, the surface remained spherical and irregular while their bases were plastically deformed upon impact to form bonding with prior coatings. With the particle incidence angle reaching 90°, particle variables occur only in the thickness direction, and the amount of spherical particles observed on the coating surface. As the incidence angle decreased, the particle deformed due to horizontal shear force, resulting in less spherical particles.

Figure 5 illustrates the schematic drawing of 60° and 90° incident Cu particles. Assuming the particle velocity is V. With the incident angle of 90°, the substrate experiences severe plastic deformation and the Cu particles impact deeply into the
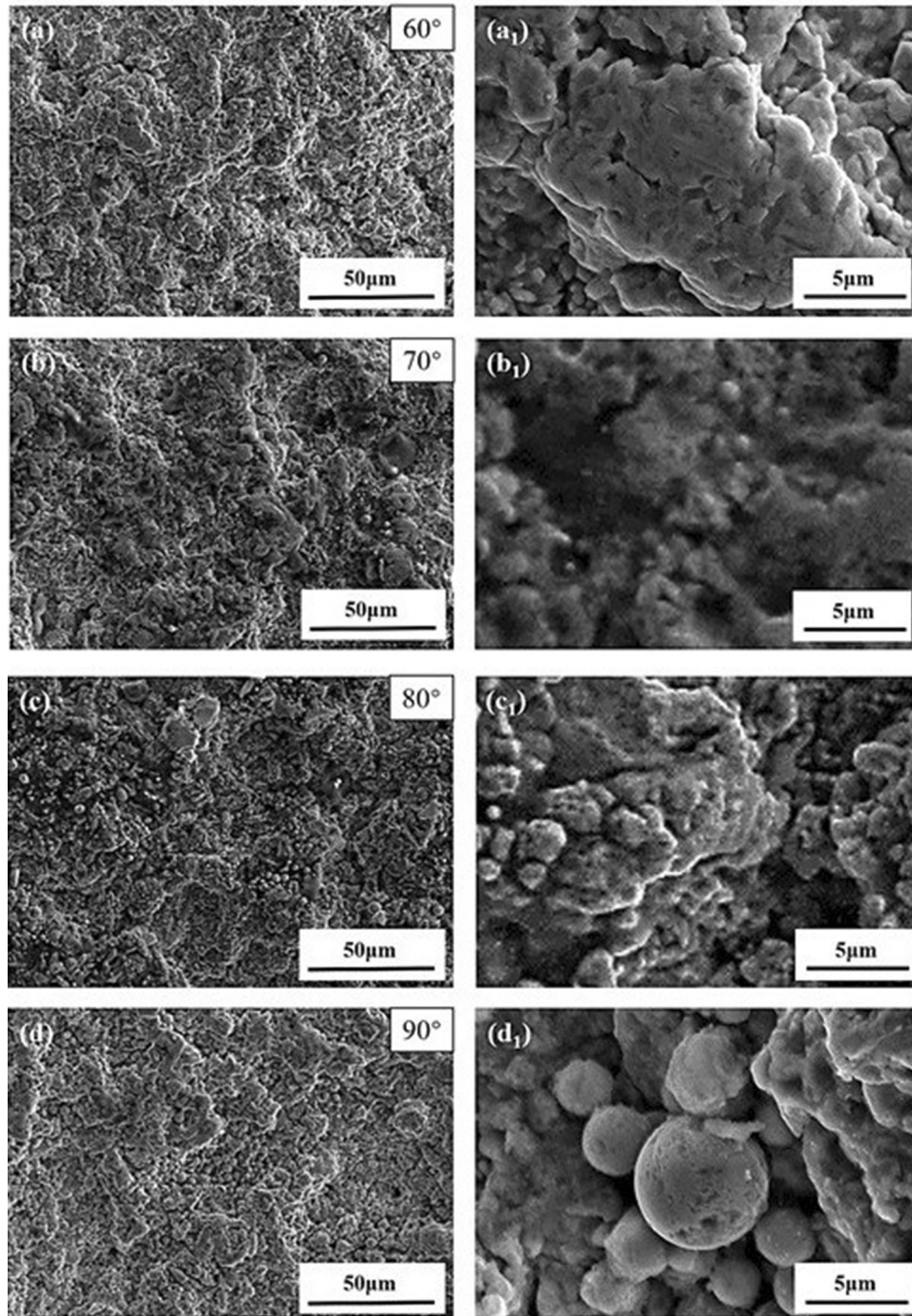

Fig. 4 SEM images of the Cu surfaces from the coating of different particle incident angles. (a) and (a₁) 60°. (b) and (b₁) 70°. (c) and (c₁) 80°. (d) and (d₁) 90°
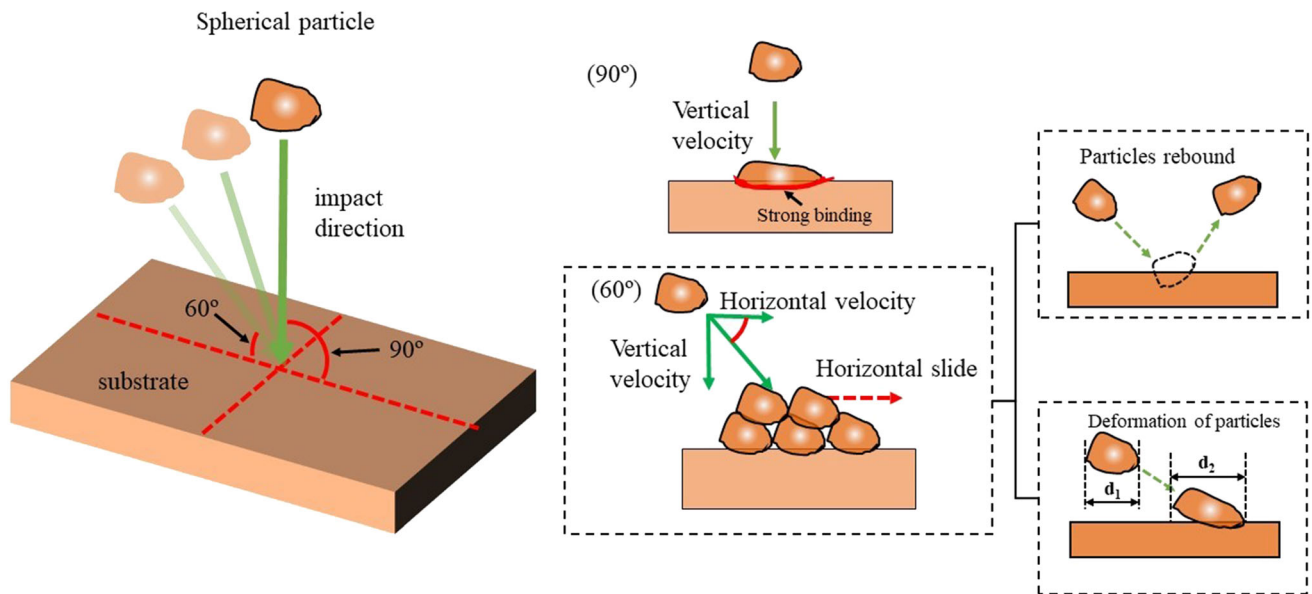
Fig. 5 Schematic drawing of different angles of incident Cu particles
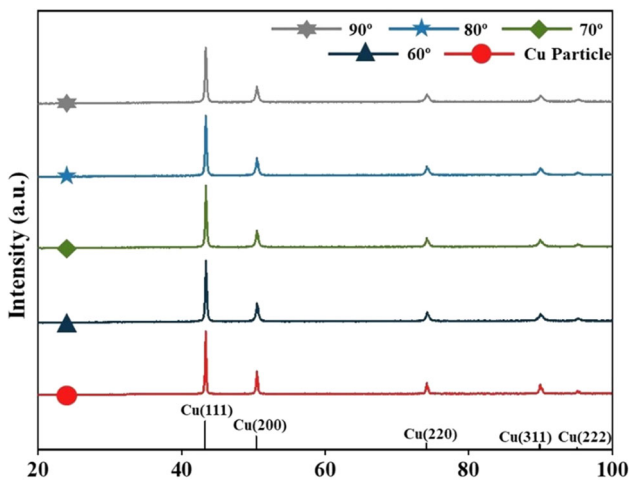

Fig. 6 XRD patterns from the as-received Cu powders and coating of different particle incidence angles

substrate at normal spray angle (V = Vertical velocity). With the incident angle of 60°, the particle velocity can be decomposed into a vertical velocity and horizontal velocity, since the main binding mechanism of cold spraying is due to the mechanical interlocking effect between particles (Ref 10). With the incident angle of 60°, the vertical kinetic energy is reduced due to the decrease of the vertical velocity, so that some relatively small particles are bounced off, reducing the deposition efficiency of particles. Due to the horizontal velocity, the particle slides along the direction of impact and penetrates less deeply and has horizontal shear force and deformation ($d_2 > d_1$).

Figure 6 shows the XRD patterns from as-received Cu powders and coatings. No significant changes in phases or oxide formation appears after the particle deposition. It has been noted that such result was found because cold spraying is performed at low temperature. Therefore, there were no changes in the material compositions and the coatings obtained were homogeneous and almost oxide-free (Ref 26, 27). And residual stress of coating with different incident angles is shown in Table 1. (The diffraction line displacement is measured by x-ray diffraction measurement method as the original data, and the measured result is the residual strain, and then the residual stress is calculated by Hooker's law.) It can be seen that normal stresses dominate the final residual stresses. After the coatings have been completed, the resulting residual stress state in the Cu coatings is compressive in all cases, because cold spraying is a method using plastic deformation of powders rather than a heat source used in other thermal spray processes. As Fig. 5 shows, particles' velocity can be decomposed into a vertical velocity and horizontal velocity. Particles' horizontal velocity increased with the incident angle decreased. Due to the horizontal velocity, the particle slides along the direction of impact. Because the particles slide along the impact direction, the coating generates a shear stress, and the shear stress increases with the increase of horizontal velocity. In order to distinguish the residual stress situation at the top and bottom of the coating, we selected the sample with the particle incidence angle of 90° for residual stress analysis. The top and bottom of the coating are both residual compression (Ref 18, 28). The residual compressive stress at the top of the coating is 334 MPa, while the residual compressive stress at the bottom of the coating has increased to 433 MPa, while the shear stress has not changed significantly. This is due to the impacting effect of subsequent particles on the deposited particles, which led to the accumulation of compressive stress in the deposited coating, and finally formed the situation of elevated residual compressive stress at the bottom.

High-magnification EBSD scans for the coatings of 90° are shown in Fig. 7. The indexing is not existing in the splat boundary area, demonstrating that severely deformed strained

Table 1 Residual stress of Cu coatings from XRD.

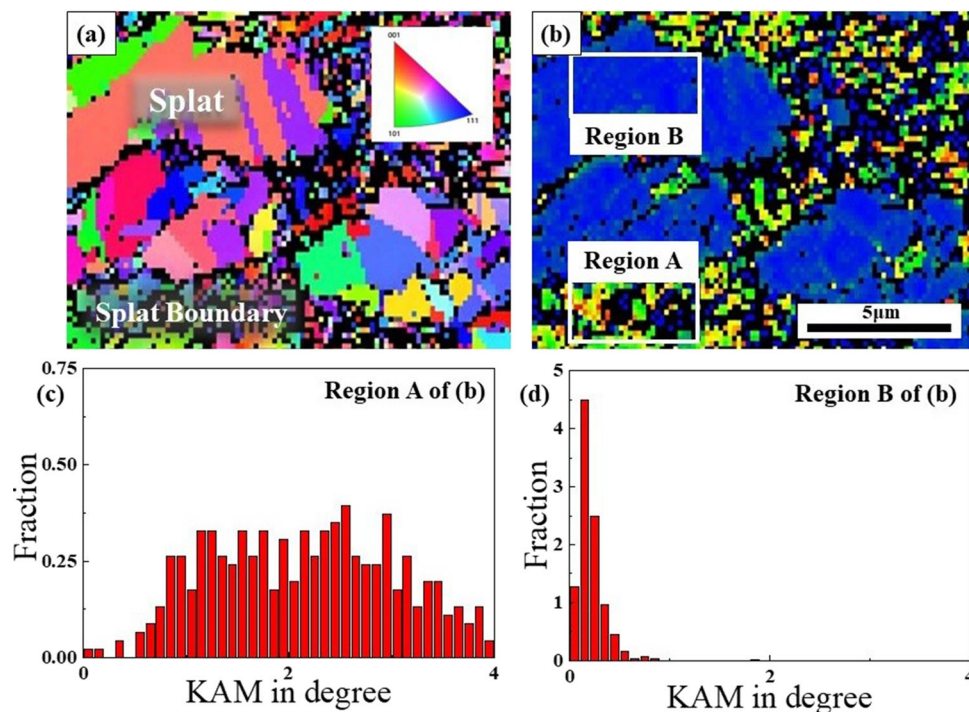|	90º	80º	70º	60º
Normal stress (MPa)	− 334.8 ± 27.5	− 349.6 ± 36.3	− 320.6 ± 50.7	− 286.9 ± 51.5
Shear stress (MPa)	− 5.0 ± 4.7	− 7.6 ± 8.7	− 17.5 ± 6.2	− 15.0 ± 8.2

Fig. 7 EBSD of cross section for the coatings of 90º: (a) inverse pole figure (IPF) maps, (b) kernel average misorientation (KAM) maps (c & d) Region KAM fraction of Fig. 7(b)

region appears in the well bonded and coalesced particles (Fig. 7a). Besides, the formation of non-indexed regions at splat boundaries is ascribed to the existence of nano-grains due to the high-velocity particle impact (Ref 29, 30). The KAM values in different regions are calculated in Fig. 7(b), (c) and (d). The lower KAM values (<2º) correspond to splats, while the higher KAM values (>2º) correspond to splat boundaries, representing a large strain exists among the nano-grains (Ref 5) .

Figure 8 shows EBSD of cross section for the coatings of 60º and 90 º. As we can see from Fig. 8, different incident angles have little influence on the main distribution of KAM values in the coating. (The lower KAM values (<2º) correspond to splats, while the higher KAM values (>2º) correspond to splat boundaries.) The main difference is the deformation degree of particles. With the incident angle of 90º (Fig. 8a2), the deformation degree of particles is obviously greater than that of 60º (Fig. 8a1). This is due to the different vertical velocity and the different compressive stress generated during the particles impact, which leads to the change of the deformation of the particles in the coating.

Figure 9 shows the morphology of cross section for the coatings. With increasing incident angles, the vertical velocity increases slightly, which improves the particle deposition efficiency, and the coating thickness increases as well. The maximum coating thickness (186.4 μm) is attained at 90° particle incident angle (Fig. 9d). Compared with 60º, it is improved by 42.7% (Fig. 9a-d). With the vertical velocity decreasing to a certain value (the angle lower than 70º), the pores can be seen in the static morphology (Fig. 9a1-d1). And the EDS of cross section shows the content of Cu element in the coating is almost 100%. This result shows the advantages of cold spraying, which does not cause any oxides furthermore (Ref 26).

Figure 10 shows the morphology of cross section for the coatings of 90º and 60º. With the incidence angles of 90º, the close contact of coatings in Fig. 10(a1) appears a high density without obvious cracks or delamination. Region A of coating is observed in a high-magnification morphology (Fig. 10b1), in which the almost particles have slight deformations. Two sides exist there as shown in Fig. 10(c), including the bottom of the coating and the top of the coating. The amount of pores is increased in the vertical direction (Fig. 10d1). Almost no pores are observed at the bottom of the coating, while a large amount of pores appears at the top of the coating. With the incidence angles of 60º, the amount of pores is also increased in vertical direction (Fig. 10d2). However, it can be seen in Fig. 10(d1) and (d2) that the size and number of pores at incident angle of 60º are significantly higher than incident angle of 90º.
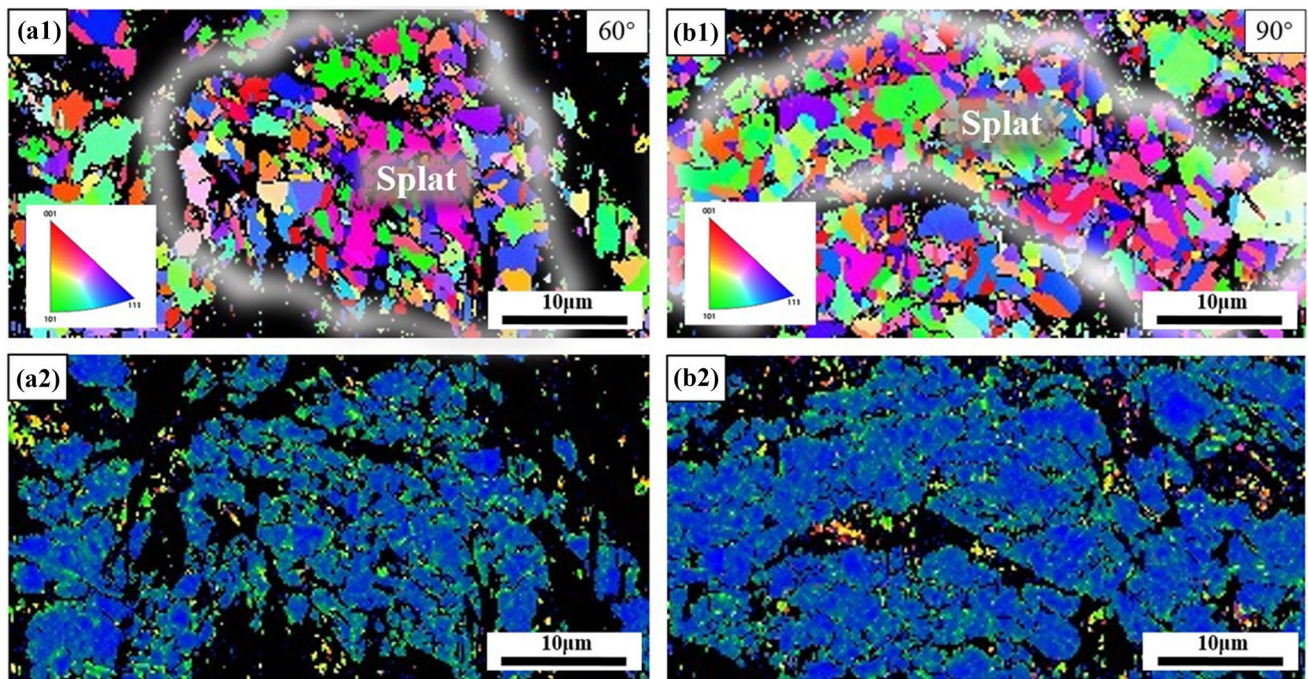
Fig. 8 EBSD of cross section for the coatings of 60° and 90° (a_1 & b_1) inverse pole figure (IPF) maps (a_2 & b_2) Kernel average misorientation (KAM) maps

Figure 11 illustrates the schematic of Cu powder particle impacting along vertical direction. During particle deposition, the bottom of the coating is preferentially impacted. The plastic deformation of the particles at the bottom of the coating is increased due to the impact effect of a large number of subsequent particles, making the bottom of the coating more compact (Fig. $10c1_{\&2}$ and $d1_{\&2}$), which is similar to shot peening (Ref 30). As the deposition process goes on, the amount of particles is gradually reduced (Fig. 11). The reduction of particle number affects the re-plastic deformation of deposited particles. And the pores gradually appear between the particles, resulting in the porosity (Fig. $10d1_{\&2}$). Finally, the plastic deformation degree of the particles decreases in the surface area of the coating because there is almost no subsequent particles, and some of particles almost keep original shapes (Fig. $10b1_{\&2}$).

Figure 12 shows the distribution of the pores under the difference particle incidence angles, which are taken in the middle of the whole coating's cross section with SEM. The porosity of the coating is the lowest with 0.8% with the particle incident angle reaching 90º (Fig. 12a). With the decrease of particle incidence angles, the number of pores increases continuously, resulting in higher porosity. The porosity of the coating reaches to 5.32% when the particle incident angle reaches 60º (Fig. 12d). And it can be seen that the number of pores increases continuously in vertical direction, which is consistent with the results in Fig. $10d1_{\&2}$.

Lower porosity of cold-sprayed Cu coating due to continuous high-velocity impact of dense Cu particles results in densification of deposited coating (Ref 31). The values of Vickers hardness are shown in Fig. 13. The hardness of the coating has been analyzed in the direction parallel to and perpendicular to the interface. A minimum of ten measurements

of each sample are measured in order to derive the standard deviation as error bars in Fig. 13. The hardness value of the substrate is basically stable at 160-165 HV, which is consistent with the hardness value of conventional Cr-Zr-Cu alloy. At the bottom of the coating, the hardness value is higher than 120 HV (Fig. 13a). But at the top of the coating, the hardness of the coating decreases (below 120 HV) due to the increase of porosity. Similar results are obtained by comparing the curves of 60° particles incident angle. The hardness of the coating decreases with the decrease of the particle incident angle (Fig. 13b). In the curves of 60° particles incident angle, obvious crack extension occurs with the application of load.

The nano-hardness and modulus are shown in Fig. 14a. The results show that the changing trend is consistent with the Vickers-hardness value. With the increase of the particle incident angles, the Nano-hardness and Young's modulus of the coating gradually all increase and reach the highest value at 90° (nano-hardness of 2.3384 GPa and Young's modulus of 138.95 GPa). The nano-hardness at the bottom of the coating is obviously higher than that at the top of the coating. This indicates that with the increase of porosity, the density of the coating decreases, resulting in the performance of the coating. While the friction coefficients of as-sprayed Cu coating with 90° also verifies the above analysis. In Fig. 14b, it can be seen that the average coefficient of friction and wear extent at the bottom of the coating is similar to that of the substrate, while the friction coefficient at the top of the coating decreases slightly and the wear increases obviously from 0.1 to 2.6 mg.

The thermal conductivity of the sample was measured with the same thickness of coating at different particle incident angles at 25 and 100 °C, respectively (Fig. 15), and compared of the Cr-Zr-Cu alloy substrate without coating (at least five points were taken in each sample to measure the thermal
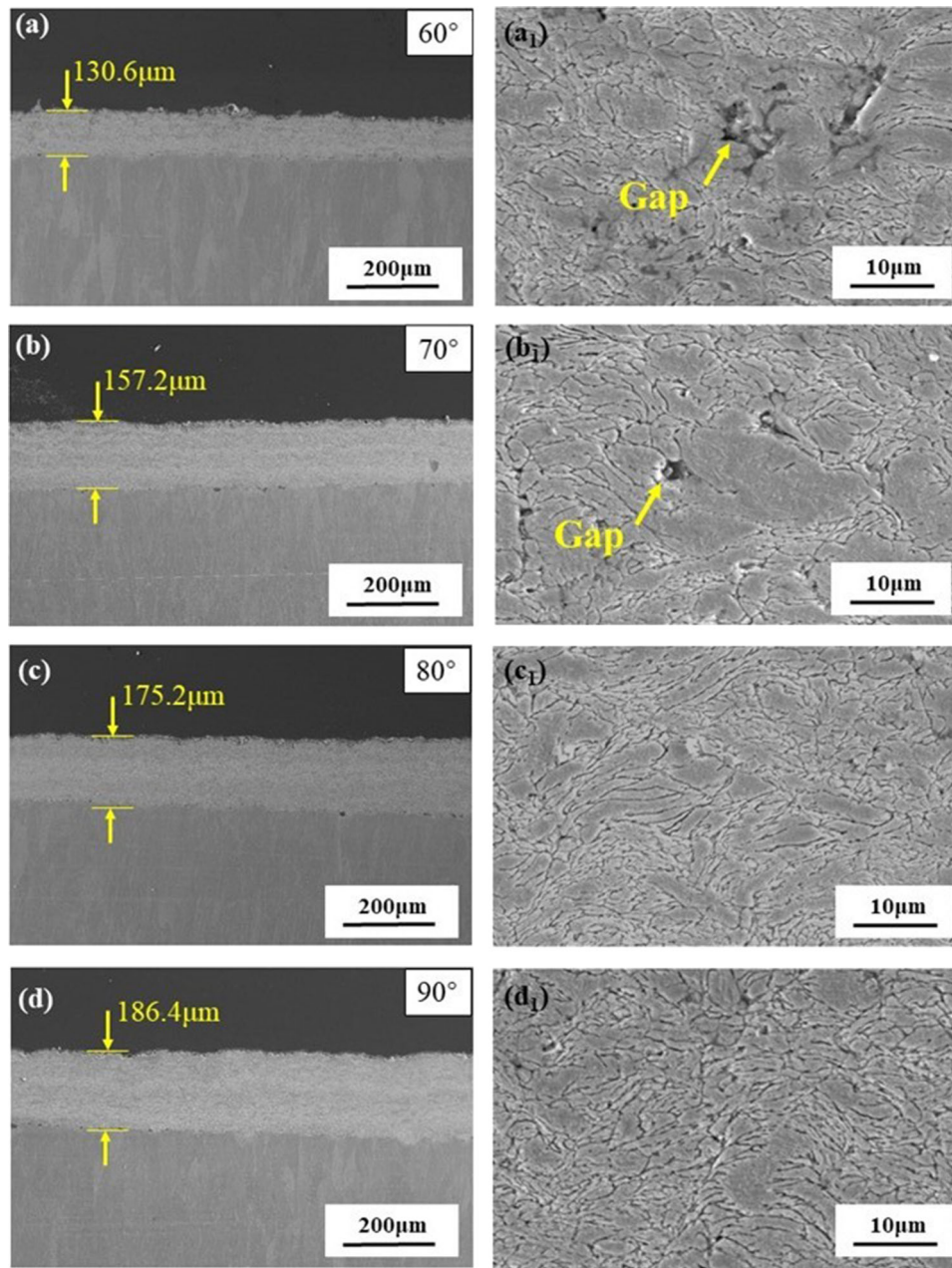
Fig. 9 The morphology of cross section for the coatings. (a-d) SEM diagram of macroscopic morphology, (a_1-d_1) SEM diagram of microscopic morphology

conductivity and take the average value, and the error bar was obtained). The thermal conductivity of the substrate at 25 and 100 °C is 324 W/m·K and 354 W/m·K, respectively. The thermal conductivity of the sample increases with the increase of spraying angle. When the particle incident angle is 90°, the thermal conductivity of the sample is the highest, reaching 95.3% of the substrate, which reaches 90.7% of the pure copper block (Ref 32). However, with the increase of temperature, this ratio decreases (the thermal conductivity reaches 89.8% of the substrate at 100 °C).

4. Conclusion

In summary, the influence of particles incident angle in a range of 60° to 90° on properties of Cu coatings on Cr-Zr-Cu substrate via high-pressure cold spray was investigated.

The low porosity and high deposition efficiency of the Cu coatings are achieved with the increment of particles incident angle due to the high normal velocity and high-velocity particle impact. The bottom of the coating is preferentially impacted,
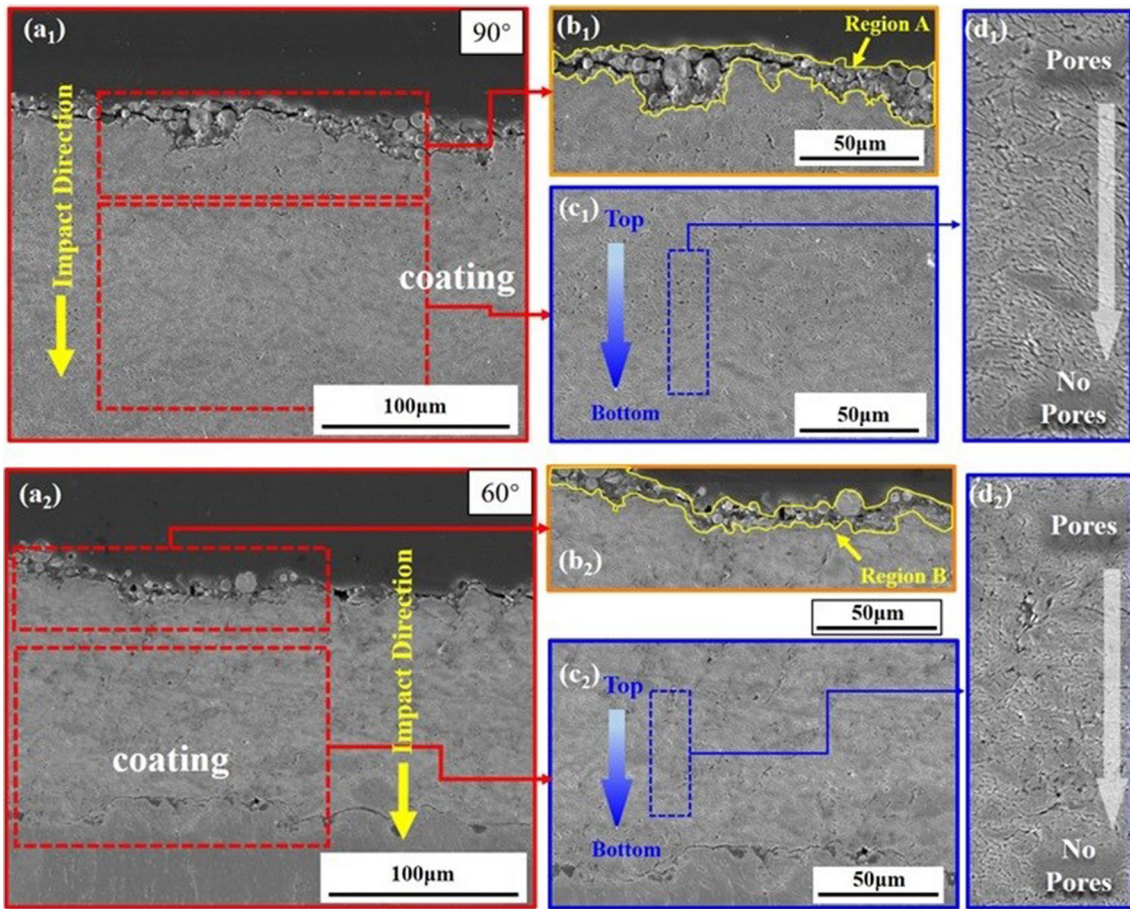
Fig. 10 SEM of cross section for the coatings of 90° and 60°. (a) Low-magnification SEM of cross section for the coatings. (b) Region I of Fig. 9(a). (c) Region II of Fig. 9(a). (d) High-magnification SEM of cross section for the coatings.
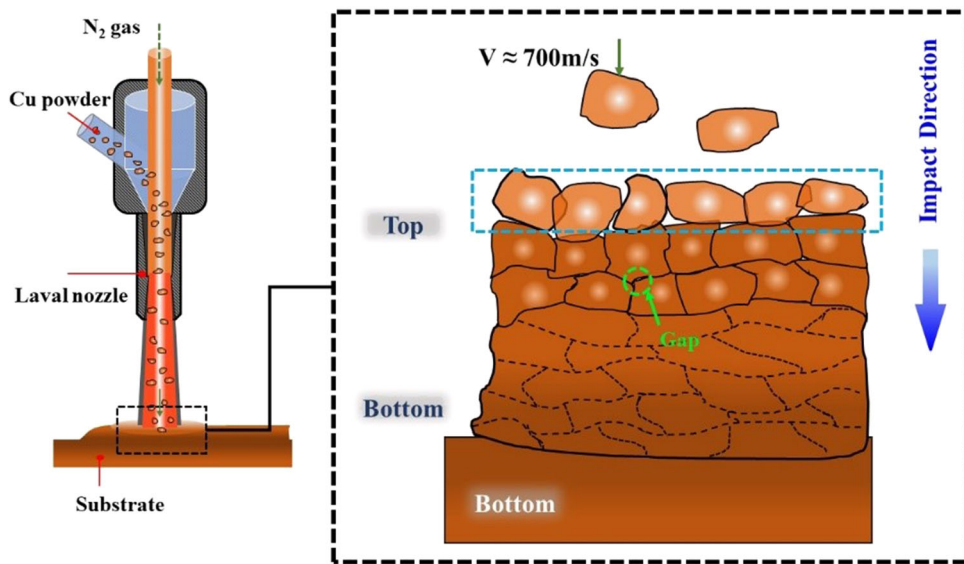

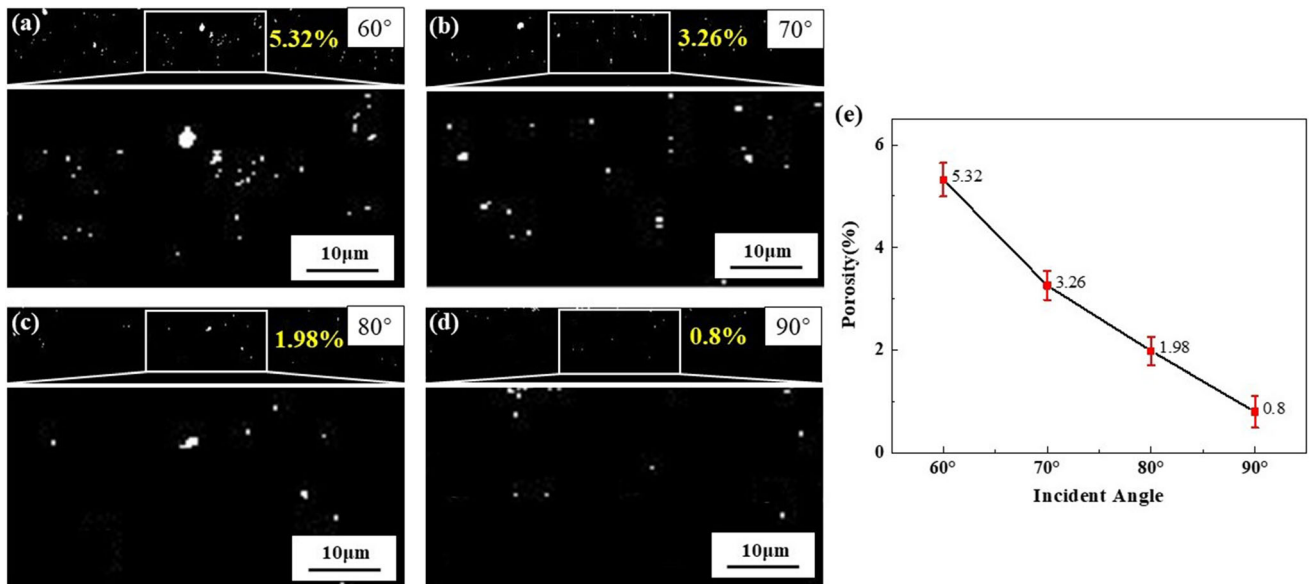**Fig. 11** Schematic drawing of Cu powder particle impacting along vertical direction

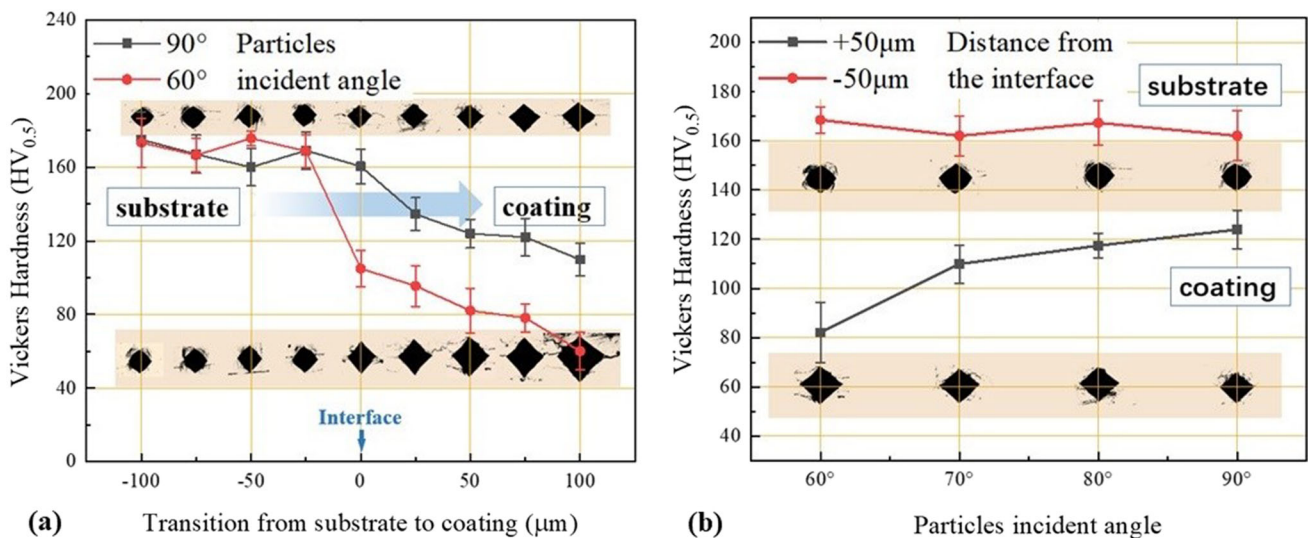**Fig. 12** Coating porosity of different particle incident angles

Fig. 13 (a) Coating hardness along the vertical interface of different particle incident angles (90°, 60°). (b) Coating hardness at the same level (50 μm from the interface) of different particle incident angles

resulting in the plastic deformation and compaction of the bottom particles. The impact for the top of the coating is reduced, leading to the small re-plastic deformation and the appearance of pores.

The thickness of Cu coatings is increased by 42.7% at 90° incident angle compared to that of 60°. The high Vickers-hardness of Cu coatings is 120 HV, reaching 82.7% of Cr-Zr-
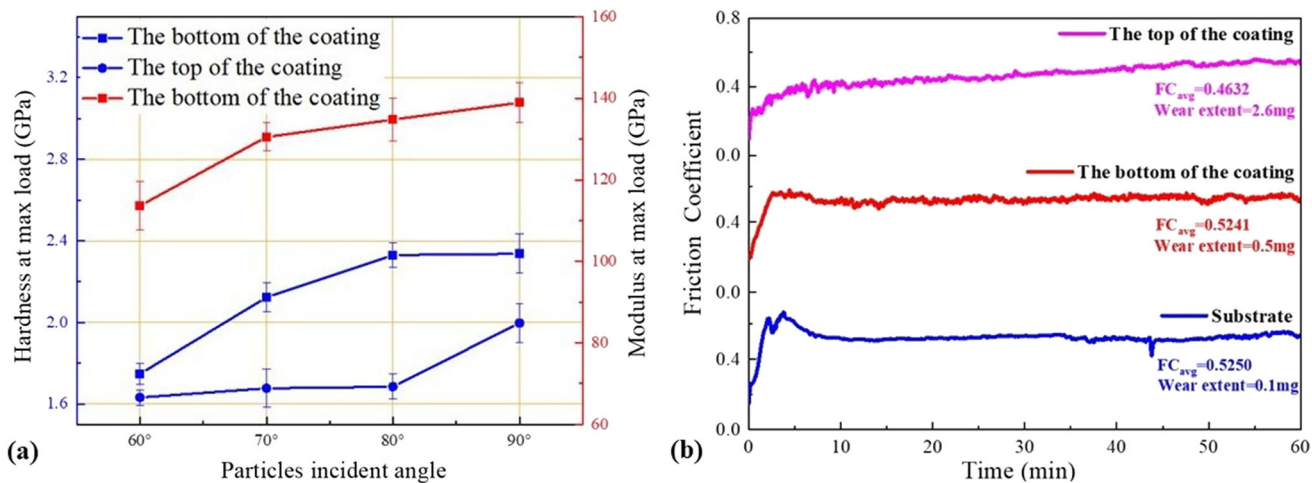
Fig. 14 (a) Coating hardness and modulus of different particle incident angles. (b) Coating friction coefficient in different areas of 90° particle incident angles
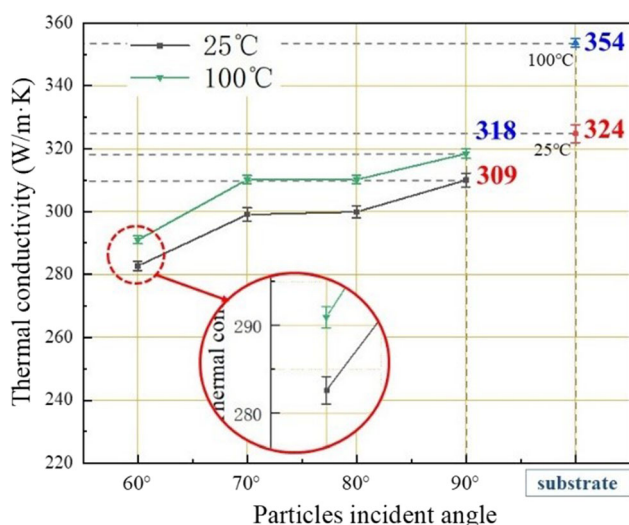

Fig. 15 Coating thermal conductivity of different particle incident angles (25 and 100 °C)

Cu substrate. It is attributed to the low porosity of 0.8% and the deformation strengthening of pure Cu particles.

Data availability

Data openly available in a public repository.

Conflict of interest

The authors declare that there is no conflict of interests; we do not have any possible conflicts of interest.

References

1. S. Zhou, B. Zhao, Z. Zhen et al., Application of Lanthanum in High Strength and High Conductivity Copper Alloys, *J. Rare Earths*, 2006, **24**(1), p 385–388.
2. I. Yasar, A. Ca Nakci and F. Arslan, The Effect of Brush Spring Pressure on the Wear Behaviour of Copper–Graphite Brushes with Electrical Current, *Tribol. Int.*, 2007, **40**(9), p 1381–1386.
3. A.P. Alkhimov, A.N. Papyrin, V.F. Kosarev, et al. Gas-Dynamic Spraying Method for Applying a Coating: US, US5302414 A[P]. (1997)
4. A.N. Papyrin, V.F. Kosarev, S.V. Klinkov, et al. On the Interaction of High Speed Particles with a Substrate under the Cold Spraying. (2002)
5. H. Assadi, Klassen, et al., Cold Spraying—A Materials Perspective, *Acta Mater.*, 2016, **116**, p 382–407.
6. S. Yin, P. Ca Valiere, B. Aldwell et al., Cold Spray Additive Manufacturing and Repair: Fundamentals and Applications, *Addit. Manuf.*, 2018, **21**, p 628–650.
7. W. Li, K. Yang, S. Yin et al., Solid-State Additive Manufacturing and Repairing by Cold Spraying: A Review, *J. Mater. Sci. Technol.*, 2018, **34**(3), p 440–457.
8. W. Li, C. Cao and S. Yin, Solid-State Cold Spraying of Ti and its Alloys: A Literature Review, *Progress Mater. Sci.*, 2020, **110**(11), p 100633.1-100633.53.
9. W. Li, H. Assadi, F. Gaertner et al., A Review of Advanced Composite and Nanostructured Coatings by Solid-State Cold Spraying Process, *Crit. Rev. Solid State Mater. Sci.*, 2019, **44**(2), p 109–156.
10. F. Raletz et al., Critical Particle Velocity under Cold Spray Conditions, *Surface Coat. Technol.*, 2006, **201**(5), p 1942–1947.
11. T. Schmidt, F. Gartner, H. Assadi et al., Development of a Generalized Parameter Window for Cold Spray Deposition, *Acta Mater.*, 2006, **54**(3), p 729–742.
12. M. Grujicic, C.L. Zhao, W.S. Derosset et al., Adiabatic Shear Instability Based Mechanism for Particles/Substrate Bonding in the Cold-Gas Dynamic-Spray Process, *Mater. Des.*, 2004, **25**(8), p 681–688.
13. H. Koivuluoto, A. Coleman, K. Murray et al., High Pressure Cold Sprayed (HPCS) and Low Pressure Cold Sprayed (LPCS) Coatings Prepared from OFHC Cu Feedstock: Overview from Powder Characteristics to Coating Properties, *J. Therm. Spray Technol.*, 2012, **21**(5), p 1065–1075.
14. M.R. Rokni, C.A. Widener and V.R. Champagne, Microstructural Evolution of 6061 Aluminum Gas-Atomized Powder and High-Pressure Cold-Sprayed Deposition, *J. Therm. Spray Technol.*, 2014, **23**(3), p 514–524.
15. G. Jeandin, et al. Influence of spray angle on cold spray with Al for the repair of aircraft components. *Dvs Berichte* (2014)
16. Z. Zhang, D. Leng, M. Lin et al., Cold Spray Deposition of Inconel 718 in Comparison with Atmospheric Plasma Spray Deposition, *Appl. Surface Sci.*, 2020, **535**, p 147704.

17. R. Singh, K.H. Rauwald, E. Wessel et al., Effects of Substrate Roughness and Spray-Angle on Deposition Behavior of Cold-Sprayed Inconel 718, *Surf. Coat. Technol.*, 2017, **319**, p 249–259.

18. E. Lin, Q. Chen, O.C. Ozdemir et al., Effects of Interface Bonding on the Residual Stresses in Cold-Sprayed Al-6061: A Numerical Investigation, *J. Therm. Spray Technol.*, 2019, **28**, p 472–483.

19. W. Wong, A. Rezaeian, E. Irissou et al., Cold Spray Characteristics of Commercially Pure Ti and Ti-6Al-4V, *Adv. Mater. Res.*, 2010, **89–91**, p 639–644.

20. S. Yin, X. Suo, J. Su et al., Effects of Substrate Hardness and Spray Angle on the Deposition Behavior of Cold-Sprayed Ti Particles, *J. Therm. Spray Technol.*, 2014, **23**(1), p 76–83.

21. L.I. Wenya, L.I. Changjiu, W. Yuyue et al., Effect of Parameters of Cold Sprayed Cu Particles on its Impacting Behavior, *Acta Metall. Sin.*, 2005, **41**(3), p 282–286. (**(in Chinese)**)

22. C.H. Ng, S. Yin, R. Lupoi et al., Mechanical Reliability Modification of Metal Matrix Composite Coatings by Adding Al Particles via Cold Spray Technology, *Surfaces Interfaces*, 2020, **20**, p 100515.

23. A. Xtl, G.A. Yi, B. Yx et al., Dynamic Evolution of Oxide Scale on the Surfaces of Feed Stock Particles from Cracking and Segmenting to Peel-Off While Cold Spraying Copper Powder Having a High Oxygen Content, *J. Mater. Sci. Technol.*, 2021, **67**, p 105–115.

24. V. Munagala, R. Chakrabarty, J. Song et al., Effect of Metal Powder Properties on the Deposition Characteristics of Cold-Sprayed Ti6Al4V-TiC Coatings: An Experimental and Finite Element Study, *Surfaces Interfaces*, 2021, **25**, p 101208.

25. Y. Xie, C. Chen, M.P. Planche et al., Effect of Spray Angle on Ni Particle Deposition Behaviour in Cold Spray, *Surface Eng.*, 2017, **34**(5), p 352–360.

26. B.V. Padmini, D.G. Bhosale and H.B. Niranjan, A Study of T11 Boiler Steel Protection by Cold Sprayed Inconel 738 Coating Against High Temperature Erosion, *Surfaces Interfaces*, 2021, **23**, p 101002.

27. Z. Zhang, H.L.D. Seng, M. Lin, S.L. Teo, T.L. Meng, J.J.C. Lee, Z.-Q. Zhang, T. Ba, J. Guo, K. Sundaravadivelu, P.K. Aw and J. Pan, Cold Spray Deposition of Inconel 718 in Comparison with Atmospheric Plasma Spray Deposition, *Appl. Surf. Sci.*, 2021, **535**, p 147704.

28. R. Ghelichi, S. Bagherifard, D. Macdonald et al., Experimental and Numerical Study of Residual Stress Evolution in Cold Spray Coating, *Appl. Surface Sci.*, 2014, **288**(JAN. 1), p 26–33.

29. J.Y. Lek, A. Bhowmik, A.W.-Y. Tan, W. Sun, X. Song, W. Zhai, P.J. Buenconsejo, F. Li, E. Liu, Y.M. Lam and C.B. Boothroyd, Understanding the Microstructural Evolution of Cold Sprayed Ti-6Al-4V Coatings on Ti-6Al-4V Substrates, *Appl. Surf. Sci.*, 2018, **459**, p 492–504.

30. X.T. Luo, Y.K. Wei, Y. Wang et al., Microstructure and Mechanical Property of Ti and Ti$_6$Al$_4$V Prepared by an In-Situ Shot Peening Assisted Cold Spraying, *Mater. Des.*, 2015, **85**(Nov. 15), p 527–533.

31. F. Sevillano, P. Poza, C.J. Mu'nez, S. Vezzu, S. Rech and A. Trentin, Cold-Sprayed Ni-Al$_2$O$_3$ Coatings for Applications in Power Generation Industry, *J. Therm. Spray Technol.*, 2013, **22**, p 772–782.

32. K. Cao, M. Yu, C.M. Liang and H. Chen, Study on Thermal Conductivity of Cold Sprayed Cu Coating, *Surf. Eng.*, 2020, **36**(10), p 1058–1066.